Source Apportionment of $PM_{2.5}$ Trace Elements at an Urban Site in Bangkok, Thailand

Lin Myat Hein[1], Saran Salakij[2], Mushtaq Ahmad[3,4], Phailin Thaveevong[1], Anucha Fueangfung[1], and Sirima Panyametheekul[1,5*]

[1]Department of Environmental and Sustainable Engineering, Faculty of Engineering, Chulalongkorn University, Bangkok 10330, Thailand
[2]Department of Mechanical Engineering, Faculty of Engineering, Chulalongkorn University, Bangkok 10330, Thailand
[3]Department of Space Sciences, School of Sciences, Institute of Space Technology, Islamabad 44000, Pakistan
[4]Atmospheric Science Research Unit: National Astronomical Research Institute of Thailand, Chiang Mai, 50180, Thailand
[5]Energy Research Institute, Chulalongkorn University, Bangkok 10330, Thailand
**Corresponding Author E-mail: sirima.p@chula.ac.th*

ABSTRACT

Fine particulate matter ($PM_{2.5}$) in Bangkok exhibits strong seasonal variation, but source apportionment studies in the region have largely been confined to the dry season, leaving the stability of source contributions across the monsoon cycle uncharacterized. In this study, $PM_{2.5}$ mass and $PM_{2.5}$-bound elements were measured at hourly resolution using an automated energy-dispersive X-ray fluorescence analyzer (PX-375) at an urban site in central Bangkok. The measurement campaign was conducted for two months during each season: the dry season (December 2024–January 2025) and the wet season (July–August 2025). EPA PMF 5.0 was used to identify the potential sources of $PM_{2.5}$-bound metal elements in urban Bangkok. Mean $PM_{2.5}$ concentration was 33.9 μg m^{-3} in the dry season and 11.0 μg m^{-3} in the wet season, a significant threefold difference (Mann-Whitney U test, $p < 0.001$). K, S and Rb were enhanced 3.8- to 4.6-fold in the dry season, whereas Cu and Ni showed no enhancement. Four factors were resolved during the dry season and three during the wet season. A mixed traffic-related non-exhaust and fuel-oil combustion factor contributed similarly in both seasons (13.8% of the modelled elemental mass in the dry season and 14.9% in the wet season) and was among the better-constrained factors in each solution. Crustal and road-dust material was resolved as a separate factor only during the monsoon, although this factor was the least uniquely determined of the wet-season solution. These results indicate the persistent influence of local traffic emissions throughout the year, while highlighting that the degree to which individual sources can be separated by receptor modelling is itself seasonally dependent.

Keywords: X-ray fluorescence/ Traffic emission/ Urbanization source apportionment/ Health risk

1. INTRODUCTION

Fine particulate matter also known as $PM_{2.5}$ is the air pollutant most consistently linked to adverse health outcomes, contributing an estimated 4.1 million premature deaths annually worldwide [1]. The 2021 WHO Global Air Quality Guidelines lowered the recommended annual mean concentration for $PM_{2.5}$ from 10 to 5 μgm^{-3} and the 24-hour mean concentration from 25 to 15 μgm^{-3}, reflecting stronger evidence of health effects occurring even at lower exposure levels [2]. Despite these stricter guidelines, most urban populations remain exposed to concentrations exceeding recommended levels. Health effects depend not only on mass concentration but on chemical composition, making source-resolved characterization essential for effective control [3, 4].

Although secondary inorganic ions and carbonaceous material dominate $PM_{2.5}$ mass, they are of limited value for identifying specific emission sources, as they arise from multiple pathways and are altered by atmospheric transformation. Trace elements are therefore widely used in source apportionment because they preserve characteristic source signatures [5]. Their relative abundances reflect the composition of parent materials, including crustal minerals, fuel components, and industrial additives, and many refractory elements remain chemically stable during atmospheric transport, so the proportions observed at a receptor site remain close to those at emission. Energy-dispersive X-ray

fluorescence (EDXRF) further enables simultaneous, non-destructive measurement of a wide suite of elements, providing both the number of variables required by multivariate receptor models such as positive matrix factorization (PMF) and, in automated instruments, the temporal resolution needed to examine seasonal variability.

However, no single element serves as an exclusive source marker. Potassium can originate from both biomass and coal combustion, V/Ni ratios vary with fuel composition and emission controls, and Fe and Mn may derive from both crustal and traffic source [5]. Source identification therefore requires the simultaneous consideration of multiple elemental species, which is the basis for applying a receptor model that resolves sources from the covariance structure of the full elemental dataset rather than from individual markers [5-7].

Bangkok is a major $PM_{2.5}$ pollution hotspot owing to high urban density and industrial activity. The principal sources of $PM_{2.5}$ and PM_{10} include vehicle emissions, biomass burning, industrial emissions, secondary aerosol formation, coal combustion, and dust [8]. Previous source apportionment studies indicate that $PM_{2.5}$ in Bangkok is dominated by biomass burning and vehicle emissions. Dispersion modelling shows substantial contributions close to major roads, indicating that the influence of traffic is highly spatially variable; a single freeway was found to account for approximately 32% of the annual mean $PM_{2.5}$ concentration at a roadside hotspot in the central business district. High Cu and Zn concentrations, associated mainly with brake wear and tire abrasion, are a characteristic feature of traffic-related factors in receptor modelling studies, and road dust resuspension and construction activity are significant additional contributors in Bangkok [9, 10]. PMF applied to ion-beam-analyzed $PM_{2.5}$ samples collected during the COVID-19 lockdown resolved distinct source contributions across the metropolitan region: biomass and solid-waste burning dominated in Bangkok at 45.6% of $PM_{2.5}$ mass, traffic emissions were the major contributor in Samut Prakan at 43.7%, and construction-related emissions predominated in Samut Sakhon at 36.0% [11]. Biomass burning has been estimated to contribute approximately 33.9% of $PM_{2.5}$ during the dry season and 28.4% during the wet season, although its influence is strongly modulated by regional transport. Local open burning contributes relatively little to direct emissions within the Bangkok Metropolitan Region, but transboundary transport from neighboring regions, particularly Myanmar, substantially elevates concentrations during the peak burning period in March–April [12]. Secondary inorganic aerosol, formed through atmospheric oxidation of NO_X and SO_X emitted from vehicular, fossil-fuel combustion, and industrial sources, represents a further important fraction of $PM_{2.5}$ mass in the region [13]. Particulate sulfur measured by XRF therefore indexes aged and regionally transported aerosol rather than a discrete local source.

The current study investigated the concentration and seasonal variation of $PM_{2.5}$-bound metal elements in the urban area of Bangkok using hourly measurements using an automated X-ray fluorescence analyzer (PX-375). Monitoring was conducted during December 2024 to January 2025 in the dry season and July to August 2025 in the wet season. The seasonal variations in $PM_{2.5}$ and $PM_{2.5}$-bound metal elements were investigated. The sources of $PM_{2.5}$-bound elements in each season were determined using the PMF model, and the resulting source profiles were compared between seasons to assess their consistency. This study will contribute to the identification of elemental source signatures in urban Bangkok under contrasting monsoon conditions and to an improved understanding of how source contributions vary between seasons, thereby supporting the regulation of air pollution in the Bangkok Metropolitan Region.

2. METHODOLOGY

2.1 Sampling site and Instrumentation

$PM_{2.5}$ and $PM_{2.5}$-bound metal elements were measured on the rooftop of the Department of Environmental and Sustainable Engineering, Faculty of Engineering, Chulalongkorn University, Bangkok, Thailand (13.7356°N, 100.5325°E). The sampling inlet was positioned approximately 10–15 m above ground level, which provides a measurement representative of general urban conditions while

limiting the influence of immediate ground-level sources. The elevated inlet integrates emissions mixed within the urban canopy and reduces the effect of short-term localized disturbances, making the site suitable for characterizing the chemical composition and source contributions of ambient $PM_{2.5}$ in metropolitan Bangkok. Chulalongkorn University is situated within the central business district of Bangkok, surrounded by major road networks and high-density urban infrastructure. Consequently, measured $PM_{2.5}$ concentrations reflect the combined influence of local urban emissions and regional atmospheric processes.

$PM_{2.5}$ mass and $PM_{2.5}$-bound metal elements were measured at hourly resolution using a continuous particulate monitor with integrated X-ray fluorescence analysis (PX-375, Horiba Ltd., Kyoto, Japan). The instrument comprises a filter tape unit for particle collection, a mass measurement unit, and an energy-dispersive X-ray fluorescence analysis chamber, allowing mass and elemental composition to be determined on the same sample without manual handling.

Ambient air was drawn through a $PM_{2.5}$ cyclone (VSCCA, RFPS-0498–116, Mesa Labs., NJ, USA) at a flow rate of 16.7 L min^{-1}, and particles were deposited onto a filter tape (TFH-01, Horiba Ltd.) consisting of polytetrafluoroethylene reinforced with non-woven polyethylene and polyethylene terephthalate. Mass concentration was quantified during collection by a radiocarbon-based beta-ray attenuation method, using a plastic scintillator coupled to a photomultiplier tube as the detector. Following collection, the loaded portion of the tape was advanced into the analysis chamber, where elemental composition was determined by energy-dispersive X-ray fluorescence using silicon drift detectors, with irradiation at 15 and 50 kV for 4000 s per sample. Particle-free air for instrument purging was supplied through an integral high-efficiency particulate air filter. The 4000 s irradiation time is relevant to the treatment of detection limits in this study, as it differs from the nominal analysis time underlying the manufacturer's specified values (Section 2.3).

2.2 Measurement period and seasonal windows

Two sampling periods were selected from the hourly dataset to represent contrasting monsoon conditions: 1 December 2024 - 31 January 2025 for the dry season and 1 July - 31 August 2025 for the wet season. Each period consisted of 62 days, providing balanced seasonal comparisons. The selected months represent relatively stable seasonal conditions, while September and October 2025 were excluded because they correspond to the late-monsoon transition period, during which rainfall patterns and atmospheric circulation gradually shift between southwest and northeast monsoon regimes.

Seasonal selection was further constrained by data quality assessment. The April–June 2025 period was excluded following two distinct data anomalies. During April and May, K, Mg and Cd were reported at or below zero in more than 85% of hourly records, while transition metal concentrations increased by approximately one order of magnitude relative to adjacent months, with $PM_{2.5}$ mass concentrations unaffected. During June, the pattern reversed, with Ni, Cr, Cu and Co reported as zero in 29 - 72% of records compared with fewer than 7% in July and August. Both patterns were considered inconsistent with expected atmospheric variability and were attributed to instrument configuration anomalies rather than to genuine changes in aerosol composition. July and August 2025 were therefore the only months within the southwest monsoon providing continuous, internally consistent elemental data, and the wet-season analysis was restricted to that window. The two seasonal windows consequently represent the peak northeast and southwest monsoon regimes rather than the full annual cycle, and the inter-monsoon transition is not represented in this analysis.

Hourly observations were aggregated into daily 24-h sums to represent the total elemental burden during each sampling day. Days with less than 75% hourly data availability were removed, and the final dataset consisted of 62 daily samples for each season. Because the corresponding hourly uncertainties were summed in the same way (Section 2.3), concentrations and uncertainties were scaled by the same factor, so the resulting PMF solution is equivalent to that obtained using daily means. On days with

incomplete hourly coverage, the daily sum is slightly lower than 24 times the daily mean; however, this effect is minor, as more than 98% of hourly records were retained in both seasons.

2.3 Data screening and detection limits

Records with instrument alarm flags were removed before analysis. Measurements reported as zero or negative values, which occur when the fitted elemental peak area is below the spectral background, were treated as non-detects rather than as valid measurements. After quality screening, 1465 of 1488 hourly records were retained for the dry season (December 2024-January 2025) and 1482 of 1488 for the wet season (July-August 2025), corresponding to data completeness of 98.5% and 99.6%, respectively.

Detection limits (DLs) were determined using a two-step approach. Manufacturer-provided DLs were used where available and adjusted according to the measurement conditions of this study. For elements without reported manufacturer DLs, empirical DLs were calculated from the measured data. Because manufacturer DLs were based on a 500 s irradiation time, while samples in this study were measured for 4000 s, the DLs were corrected according to the inverse relationship between detection limit and the square root of counting time.

$$MDL_{4000} = MDL_{500} \times \sqrt{(500 / 4000)} = 0.3536 \times MDL_{500}$$

Manufacturer detection limits were unavailable for eight elements (P, Cl, Mg, Ag, Cd, Ba, La, and Hg). For these species, the lowest positive concentration observed within each seasonal dataset was used as an empirical detection limit. These values represent practical substitutes rather than instrumental detection limits and therefore vary between seasons, unlike the corrected manufacturer-based limits.

Detection limit substitution and uncertainty calculations were performed at the hourly resolution before daily aggregation. Concentrations below the detection limit were replaced with one-half of the corresponding limit, while measured values above the limit were retained. Uncertainties were assigned to each hourly observation following the approach described by [14]. For values above the detection limit,

$$u = \sqrt{[(EF \times c)^2 + (0.5 \times MDL)^2]}$$

where c is the hourly concentration, MDL the applicable hourly detection limit, and EF the error fraction, set to 0.1 for all species. For substituted values,

$$u = (5/6) \times MDL$$

Daily samples were then formed by summing the 24 substituted hourly concentrations, with the corresponding daily uncertainty obtained as the sum of the 24-hourly uncertainties. Uncertainties were summed linearly rather than in quadrature, on the basis that the error fraction represents a systematic calibration term correlated across the hours comprising each daily sample.

2.4 Source apportionment by positive matrix factorization

Source apportionment was performed using EPA PMF version 5.0 [6]. PMF resolves the measured concentration matrix into a specified number of factor contributions and factor profiles under a non-negativity constraint, minimizing an objective function Q in which each observation is weighted by its individual uncertainty [7]. The concentration and uncertainty matrices described in Section 2.3 were supplied as input, and the two seasons were modelled separately, each run comprising 62 daily

samples. $PM_{2.5}$ mass was not included in the input matrix, and no Total Variable was specified. The modelled elemental mass, defined as the sum of the 24 modelled species, accounted for approximately 25% (8.6 µg m^{-3}) and 28% (3.1 µg m^{-3}) of the mean $PM_{2.5}$ mass in the dry and wet seasons, respectively. The remainder consists mainly of carbonaceous material and oxygen and other counter-ions associated with the measured elements (e.g., sulfate rather than elemental S), which are not measured by XRF. Factor contributions reported in this study are therefore expressed as percentages of the modelled elemental mass, not of $PM_{2.5}$ mass.

Of the 39 measured elements, 24 were retained for source apportionment. Fifteen elements were excluded and categorized as bad (Co, Ga, Ge, Sr, Y, Pd, Ag, Cd, In, Sn, Sb, Te, Cs, Hg and Bi) on two grounds: detection below the limit in more than 40% of hourly observations, such that their values would be dominated by substitution, and measured concentrations inconsistent with those typically reported for urban $PM_{2.5}$, which indicate spectral interference or baseline offset rather than atmospheric signal. This criterion was applied consistently across both seasonal periods, so that an element excluded in either season was excluded from both, ensuring comparability between the seasonal source profiles. Twenty-three elements were categorized as strong. Arsenic was retained but categorized as weak, so that its uncertainty tripled and its influence on the solution correspondingly reduced; its signal-to-noise ratio was 2.1 in the dry season and 0.3 in the wet season, and the implications of this are addressed in Section 3.5. Signal-to-noise ratios were evaluated for all species but were not adopted as the primary selection criterion, because the uniform error fraction applied across species produced values clustered near the upper limit of the metric and therefore gave limited discrimination.

Solutions comprising three to five factors were examined for each season. For each solution, 20 base runs were performed from a user-selected random seed with no additional modelling uncertainty applied, and the run returning the lowest robust Q was retained as the base solution. The number of factors was selected on the basis of the ratio of Q(true) to its theoretical value and its behavior with increasing factor number, the physical interpretability of the resolved profiles against established elemental source signatures, the distribution of scaled residuals, and the outcome of the error estimation described below.

Uncertainty in the selected solutions was evaluated by three methods. Bootstrap resampling (BS) was performed with 100 runs using a block size of 5 and a minimum correlation coefficient of 0.6, assessed by the proportion of bootstrap factors mapping to each base factor. Displacement analysis (DISP) was applied to the modelled species and assessed by the error code returned, the resulting change in Q, and the presence of factor swaps. Combined bootstrap–displacement analysis (BS-DISP) was assessed by the proportion of cases accepted and the number of swaps in the best-fit run. Solutions returning factor swaps in DISP at the lowest dQmax level were not accepted, as such swaps indicate that the factors are not uniquely determined by the data.

A four-factor solution was selected for the dry season and a three-factor solution for the wet season. Both converged in all 20 base runs, with Q(true)/Q(expected) of 2.07 and 2.52 respectively. DISP returned an error code of zero with no factor swaps in either season and a maximum decrease in Q below 0.01%. Bootstrap mapping exceeded 92% for all dry-season factors and reached 100%, 100% and 85% for the wet-season factors. BS-DISP accepted 90% of cases for the wet season with one swap in the best-fit run, compared with 22% of cases and three swaps for the dry season. The dry-season solution is therefore less well constrained with respect to combined random and rotational uncertainty, and the interpretation in Section 3.2 is qualified accordingly.

Resolved factors were assigned to source categories on the basis of their elemental profiles, using established tracer associations: Al, Si, Ca, Ti and Fe for crustal and road dust material; K and Rb for biomass burning; Cu, Zn, Ba and Fe for traffic-related non-exhaust emissions; V and Ni for residual fuel oil combustion; and S for secondary and regionally transported aerosol. Factor profiles resolved for the two seasons were then compared to assess the extent to which source signatures were seasonally consistent.

3. RESULTS AND DISCUSSION

3.1 $PM_{2.5}$ mass and elemental concentrations

The mean $PM_{2.5}$ concentration was 33.9 ± 15.4 µg m^{-3} during the dry season and 11.0 ± 4.7 µg m^{-3} during the wet season, showing an approximately threefold seasonal difference. The dry-season average exceeded the WHO 24-hour guideline value of 15 µg m^{-3}. During the dry season, $PM_{2.5}$ concentrations were higher in January (40.4 ± 15.4 µg m^{-3}) than in December (27.3 ± 12.3 µg m^{-3}), likely due to increasing pollutant accumulation under stagnant atmospheric conditions during the northeast monsoon period. The seasonal difference in $PM_{2.5}$ concentration was statistically significant (Mann-Whitney U = 32.00, Z = −9.445, $p < 0.001$), confirming that the approximately threefold contrast reflects a genuine and robust difference in aerosol loading between the two monsoon periods rather than random sampling variability.

The dry season mean $PM_{2.5}$ concentration of 33.9 ± 15.4 µg m^{-3} was comparable to values reported in previous studies of Bangkok (Table 2). An annual spatial-wise average of 33.6 µg m^{-3} across Bangkok monitoring stations in 2018 indicated that the dry-season mean of 33.9 µg m^{-3} is consistent with the upper range of the long-term urban background, as dry-season peak concentrations are systematically higher than the annual mean [12]. The December 2024 mean (27.3 ± 12.3 µg m^{-3}) was similar to the December 2023 value of 26.7 ± 9.8 µg m^{-3} measured using the same automated XRF platform at the same site, while the January 2025 mean (40.4 ± 15.4 µg m^{-3}) was approximately 17% higher than the January 2024 value of 34.6 ± 10.3 µg m^{-3} [8]. This difference may reflect year-to-year variations in northeast monsoon conditions and regional biomass-burning activity [9]. The dry-season mean of 33.9 µg m^{-3} was higher than the 29.0 ± 9.7 µg m^{-3} reported at the urban PCD monitoring site in Bangkok, possibly because the present study focused on December and January, when $PM_{2.5}$ concentrations are generally at their seasonal peak, whereas the dry season was defined more broadly over the October 2015–March 2017 monitoring period [13]. Overall, the observed dry-season concentrations are within the range reported for Bangkok in recent years and represent the typical seasonal increase rather than an unusual episode.

The wet-season mean of 11.0 ± 4.7 µg m^{-3} was lower than values reported in previous Bangkok studies. Wet-season means of 14.7 ± 6.0 µg m^{-3} at the urban PCD site and 15.2 ± 5.3 µg m^{-3} at the AIT suburban site in Bangkok have been previously reported [13]. The lower concentration observed here is attributable to the narrower sampling window of July and August, which corresponds to the peak of the southwest monsoon when rainfall is highest and wet scavenging of aerosol particles is most effective, whereas the wet season was defined more broadly in that study to include shoulder months with transitional meteorology and higher aerosol loading [13]. The wet-season mean of 11.0 µg m^{-3} therefore reflects the intensity of peak southwest monsoon removal processes rather than an anomalously clean episode [12, 13]. Overall, the strong difference between the dry- and wet-season means demonstrates the pronounced seasonal variability of $PM_{2.5}$ at the urban Bangkok site.

Elemental concentrations showed clear seasonal differences, although the magnitude of change varied among species (Table 1). Excluding arsenic, which was modelled as a weak species (S/N 2.1 dry, 0.3 wet) and lies largely at the detection-limit substitution value in the wet season, the largest dry-season enhancements were observed for K (4.6-fold), S (4.4-fold), and Rb (3.8-fold), followed by P (2.7-fold), Al (2.5-fold), and Se (2.4-fold). In contrast, Cu and Ni were slightly higher during the wet season, while V, Zr, Cr, Si, Fe, Cl, Ti, Ba, and La showed relatively small seasonal differences (<1.5-fold). The strong dry-season increases in K (973.7 ± 504.7 ng m^{-3}) and Rb (5.7 ± 3.7 ng m^{-3}) are consistent with greater biomass-burning influence during the northeast monsoon period, when regional transport from agricultural burning areas can affect the Bangkok Metropolitan Region [11-13]. S also increased substantially (4.4-fold; 4410.8 ± 2081.6 ng m^{-3}), reflecting contributions from combustion and secondary sulfate formation [8, 13]. Se increased by 2.4-fold (3.5 ± 5.1 ng m^{-3}), consistent with greater influence from combustion sources, particularly coal and sulfur-containing fuels [4, 5].

Traffic-related elements showed limited seasonal variation. Cu averaged 14.5 ± 8.1 ng m^{-3} in the dry season and 16.5 ± 6.4 ng m^{-3} in the wet season (dry/wet ratio = 0.88), while Ni showed similar concentrations (5.6 ± 2.8 and 5.9 ± 2.7 ng m^{-3}, respectively; ratio = 0.95). Despite the substantial decrease in $PM_{2.5}$ mass during the wet season, these elements remained relatively stable, suggesting a persistent contribution from local sources. Fe and Si showed only small dry-season enhancements (ratios of 1.41 and 1.35, respectively), consistent with their mixed crustal, road dust, and construction-related sources. Overall, the seasonal pattern indicates that regional biomass burning and secondary aerosol contributed strongly to the dry-season increase in $PM_{2.5}$, while traffic-related and crustal components remained present throughout the year.

Elemental concentrations were also compared for the same calendar months one year earlier using the same automated XRF platform at the same study site [8] (Table 3). This same-month comparison provides a direct assessment of interannual variability while minimizing differences related to season and measurement method. In December, $PM_{2.5}$ concentrations were very similar between 2024 and 2023 (27.3 ± 12.3 and 26.7 ± 9.8 μg m^{-3}, respectively), as were S concentrations (+4%). However, K was 67% higher in December 2024, indicating greater biomass-burning influence despite similar $PM_{2.5}$ mass. Al and Ca were also higher by 90% and 42%, respectively, suggesting greater crustal or road-dust influence. In contrast, Cu, Ni, and V were lower in December 2024 by 48%, 44%, and 41%, respectively, indicating interannual variability in traffic- and combustion-related elemental concentrations. The January comparison showed larger differences between years. $PM_{2.5}$ was 17% higher in January 2025, while S increased by 57% (5421.4 ± 2101.0 vs 3450.0 ± 1843.1 ng m^{-3}). K increased by 151%, reaching 1117.2 ± 525.8 ng m^{-3} compared with 445.7 ± 208.1 ng m^{-3} in January 2024, suggesting substantially greater biomass-burning influence during January 2025 [11, 12]. Al and Ca also increased by 173% and 94%, respectively, while Fe increased by 22%, indicating greater crustal influence. Mn and Cr changed little between years, whereas Zn and Pb were substantially lower in January 2025 (−63% and −73%, respectively). The higher Zn and Pb concentrations reported for January 2024 may reflect episodic source influences [5, 8], although the specific source cannot be determined from elemental concentrations alone.

Overall, the interannual comparison shows relatively consistent $PM_{2.5}$ and sulfur concentrations in December, whereas January exhibited greater variability, particularly in K, S, and crustal elements. This suggests that interannual changes in dry-season $PM_{2.5}$ at the study site are strongly influenced by variations in regional biomass burning, combustion, and crustal aerosol contributions.

Table 1. Mean ± standard deviation of $PM_{2.5}$ mass (μg m^{-3}) and selected $PM_{2.5}$-bound elements (ng m^{-3}) during the dry-season (December 2024–January 2025, n = 1465) and wet-season (July–August 2025, n = 1482).

Species	Dry season	Wet season	Dry/wet ratio
$PM_{2.5}$	33.9 ± 15.4	11.0 ± 4.7	3.07
Al	920.2 ± 346.0	365.9 ± 252.2	2.51
Si	1130.8 ± 362.2	832.8 ± 744.6	1.35
S	4410.8 ± 2081.6	1013.6 ± 885.1	4.35
K	973.7 ± 504.7	211.6 ± 152.2	4.60
Ca	254.8 ± 99.7	125.8 ± 116.5	2.03
P	23.8 ± 13.2	8.8 ± 6.8	2.72
Cl	89.1 ± 43.3	63.8 ± 72.8	1.40
Mg	532.7 ± 200.1	279.7 ± 164.6	1.90
Ti	5.2 ± 2.7	3.5 ± 2.5	1.48

Table 1. Mean ± standard deviation of $PM_{2.5}$ mass (μg m^{-3}) and selected $PM_{2.5}$-bound elements (ng m^{-3}) during the dry-season (December 2024–January 2025, n = 1465) and wet-season (July–August 2025, n = 1482). (Cont.)

Species	Dry season	Wet season	Dry/wet ratio
V	2.2 ± 1.8	1.9 ± 0.6	1.17
Cr	3.5 ± 1.8	2.6 ± 1.1	1.34
Mn	8.5 ± 4.2	5.3 ± 2.7	1.61
Fe	144.1 ± 68.2	102.5 ± 73.0	1.41
Ni	5.6 ± 2.8	5.9 ± 2.7	0.95
Cu	14.5 ± 8.1	16.5 ± 6.4	0.88
Zn	38.9 ± 31.2	23.9 ± 17.5	1.63
As*	0.4 ± 2.2	0.05 ± 0.9	8.84
Se	3.5 ± 5.1	1.5 ± 1.6	2.42
Rb	5.7 ± 3.7	1.5 ± 1.4	3.83
Zr	1.4 ± 1.2	1.2 ± 1.1	1.18
Ba	21.8 ± 13.6	16.2 ± 13.6	1.34
La	12.8 ± 7.7	9.8 ± 8.1	1.30
Ce	4.0 ± 6.6	2.4 ± 2.4	1.71
Pb	9.7 ± 15.8	5.9 ± 13.7	1.63

As* was modelled as a weak species.

Table 2. Comparison of $PM_{2.5}$ concentrations with previous studies conducted in Bangkok.

Location	Period	Dry season (μg m^{-3})	Wet season (μg m^{-3})	Reference
Bangkok	Dec 2024 – Jan 2025 (dry) Jul- Aug 2025 (wet)	33.9 ± 15.4	11.0 ± 4.7	This study
Bangkok	Oct 2023 – Jan 2024	26.7 (Dec); 34.6 (Jan)	-	[8]
Bangkok	2019–2023	24.8 ± 9.1 (2019) 24.0 ± 8.6 (2020) 23.6 ± 10.5 (2021) 22.4 ± 9.1 (2022) 26.7 ± 14.1 (2023)		[9]
Bangkok	Oct 2015–Mar 2017	29	14.7 ± 6.0 (PCD) 15.2 ± 5.3 (AIT)	[13]
Bangkok	2018	33.6 (annual mean)		[12]
Bangkok	December 2021–February 2022	54.7		[11]

Table 3. Comparison of $PM_{2.5}$ (μg m^{-3}) and elemental concentrations (ng m^{-3}) between consecutive dry seasons (2023–24 vs 2024–25).

Pollutant	Dec-23	Dec-24	Change	Jan-24	Jan-25	Change
$PM_{2.5}$	26.7 ± 9.8	27.3 ± 12.3	2%	34.6 ± 10.3	40.4 ± 15.4	17%
S	3273.4 ± 1911.0	3393.3 ± 1480.3	4%	3450.0 ± 1843.1	5421.4 ± 2101.0	57%
K	496.6 ± 231.7	829.2 ± 437.8	67%	445.7 ± 208.1	1117.2 ± 525.8	151%
Al	418.2 ± 154.9	793.4 ± 289.1	90%	383.7 ± 141.3	1046.1 ± 351.9	173%
Ca	156.1 ± 48.5	221.6 ± 81.7	42%	148.0 ± 49.9	287.6 ± 104.9	94%
Fe	128.6 ± 34.7	113.5 ± 42.3	−12%	143.0 ± 58.7	174.5 ± 75.2	22%
Mn	10.2 ± 1.1	6.8 ± 3.1	−33%	10.7 ± 2.8	10.2 ± 4.5	−5%
Cu	23.8 ± 3.2	12.4 ± 7.4	−48%	23.9 ± 3.2	16.6 ± 8.2	−31%
Ni	8.8 ± 1.1	4.9 ± 2.7	−44%	9.1 ± 1.3	6.2 ± 2.7	−32%
Zn	37.4 ± 12.8	30.8 ± 19.7	−18%	126.3 ± 47.3	46.9 ± 37.8	−63%
V	2.9 ± 1.0	1.7 ± 0.8	−41%	2.0 ± 0.5	2.8 ± 2.2	40%
Cr	4.3 ± 1.2	2.9 ± 2.0	−33%	4.4 ± 1.1	4.0 ± 1.5	−9%
Pb	8.4 ± 6.1	6.9 ± 13.4	−18%	45.1 ± 10.0	12.4 ± 17.5	−73%

3.2 Source apportionment of PM2.5-bound elements in the dry season

The four resolved factors for the dry season are shown in Figure 1 and Figure 2. Factor 1 contributed 17.7% of the modelled elemental mass and was characterized by As and Pb, with 100% of the measured As and 68.2% of the measured Pb contributed to this factor. The As–Pb association is consistent with anthropogenic thermal and industrial processes, including waste combustion, metallurgical processing, and metal recycling [5, 8], and similar As–Pb associations have been reported in industrial and waste-combustion factors in Bangkok [8]. However, As was modelled as a weak species with a low signal-to-noise ratio, and this was the least well constrained factor in the dry-season solution, with its base-run profile falling outside the bootstrap interquartile range for 20 of the 24 modelled species. This factor is therefore tentatively attributed to industrial and metal processing emissions.

Factor 2 accounted for 21.6% of the modelled elemental mass and was dominated by Se, with 89.7% of measured Se attributed to this factor. Moderate contributions were also observed for Mg (28.1%), Cl (23.9%), S (22.8%), and Ca (22.1%). The strong association of Se is consistent with coal and sulfur-bearing fuel combustion, for which Se is a commonly reported tracer [4, 5]. The co-occurrence of S further supports a combustion-related source. The contributions of Mg, Ca, and Cl may reflect additional fuel combustion or mixed aerosol influences. Factor 2 was among the best constrained in the solution, with its base-run profile falling within the bootstrap interquartile range for 23 of 24 species and was assigned to coal and sulfur-bearing fuel combustion.

Factor 3 was the dominant factor, accounting for 46.9% of the modelled elemental mass. It showed substantial contributions from S (57.3%), Fe (57.7%), Zn (58.8%), Ti (55.3%), Mn (52.0%), V (51.5%), Ba (57.3%), La (57.4%), and Ce (74.4%), together with K (38.3%), Si (40.4%), and Al (36.3%). The high S contribution is consistent with secondary sulfate and regional transport during the northeast monsoon [8, 13]. The concurrent high loadings of Fe, Ti, and Mn indicate crustal and road dust contributions, as these elements are abundant in soil minerals and resuspended road material [5, 15]. The contribution of K is also consistent with biomass-burning influence during the dry season [11, 12, 16]. Because this factor contains tracers associated with several source categories, it was interpreted as mixed urban and regional aerosol, representing the combined influence of secondary aerosol, regional biomass burning, traffic-related emissions, and crustal material. Its base-run profile falls within the bootstrap interquartile range for 11 of 24 species, consistent with its interpretation as a composite

of several co-varying source signatures rather than a discrete emission source. Its large contribution indicates that this mixed aerosol was the dominant component of the dry-season elemental burden.

Factor 4 accounted for 13.8% of the modelled elemental mass and was characterized by Zr (53.3%), Ni (49.8%), Mg (44.1%), Cu (40.2%), Cr (29.9%), and V (25.6%). The contributions of Cu and Cr are consistent with traffic-related non-exhaust emissions, particularly brake and friction wear [15]. The simultaneous presence of Ni and V suggests an additional influence from residual fuel-oil combustion, for which the Ni–V association is widely used as a source indicator [17, 18]. Mg may also reflect lubricant-related emissions. Factor 4 was likewise well constrained, with its base-run profile falling within the bootstrap interquartile range for 23 of 24 species. It was interpreted as a mixed traffic-related and fuel-oil combustion source.

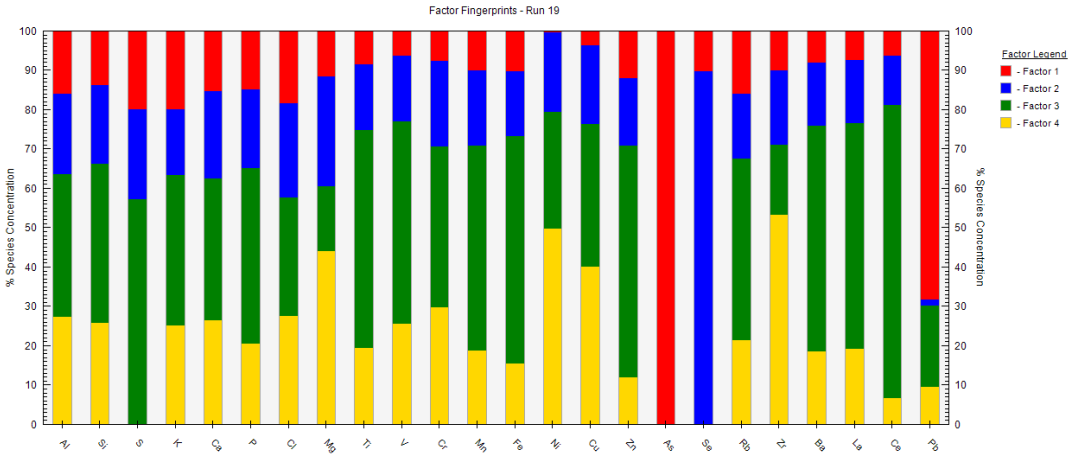

Figure 1. Factor fingerprints for the dry-season four-factor solution

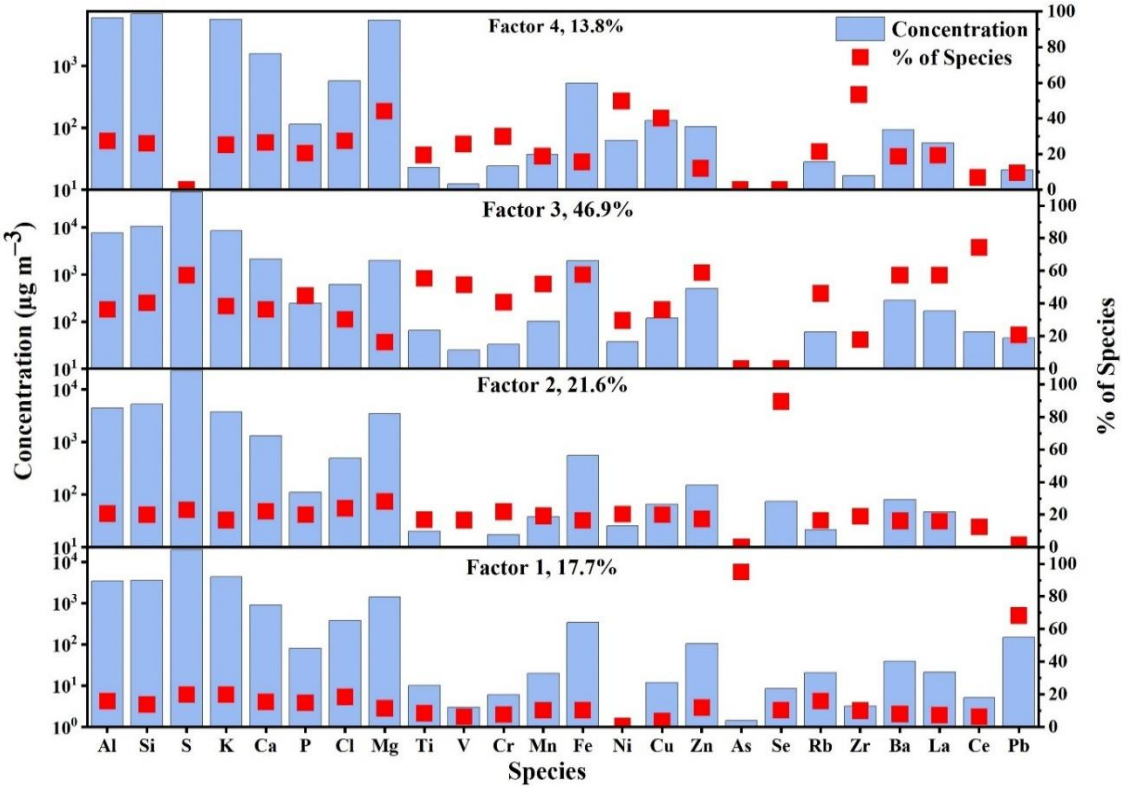

Figure 2. Source apportionment of $PM_{2.5}$ based on metal and elemental composition in the dry season using positive matrix factorization (PMF).

3.3 Source apportionment of $PM_{2.5}$-bound elements in the wet season

The three resolved factors for the wet season are shown in Figure 3 and Figure 4. The wet-season solution contained three factors compared with four in the dry season. This difference may reflect the lower $PM_{2.5}$ concentrations and weaker source contrasts during the monsoon period, when wet scavenging reduces the accumulation of secondary and regionally transported aerosol.

Factor 1 was the dominant factor, accounting for 50.0% of the modelled elemental mass. It showed contributions from a wide range of elements, including Cl (80.1%), S (55.7%), K (55.3%), Ca (54.8%), P (52.5%), Al (50.4%), and Si (47.0%), together with Mg, Pb, Ba, La, Fe, Ce, Zn, Ti, and Rb. The high Cl and Mg contributions are consistent with a marine influence during the southwest monsoon, when air masses from the Gulf of Thailand can reach the Bangkok region [13]. K and Rb indicate a residual biomass-burning contribution, while the high S contribution is consistent with secondary sulfate formation [8, 11-13]. Al, Ca, Si, Fe, and Ti indicate a crustal or road-dust component. The broad elemental profile therefore suggests contributions from several sources that were not independently resolved, and Factor 1 was consequently assigned as mixed secondary, combustion, and marine-influenced aerosol. It was the best constrained of the wet-season factors, mapping to itself in all 100 bootstrap runs, with its base-run profile falling within the bootstrap interquartile range for 19 of 24 species.

Factor 2 accounted for 14.9% of the modelled elemental mass and was characterized by Se (79.7%), Ni (76.4%), Cu (71.7%), Rb (63.7%), Cr (63.4%), V (60.5%), As (57.6%), Zn (57.0%), and Zr (55.8%), with additional contributions from Mn, Mg, and Pb. The high Cu, Cr, and Zr contributions are consistent with traffic-related non-exhaust emissions, while the Ni–V association indicates an additional influence from residual fuel-oil combustion [17, 18]. The strong Se contribution suggests a contribution from coal or sulfur-bearing fuel combustion [4, 5], while As may reflect an additional industrial or combustion component, although its wet-season concentrations were largely below the detection limit and this contribution is uncertain. Rb indicates some residual biomass-burning influence. Because several source-related signatures occur together, Factor 2 was interpreted as a mixed traffic, fuel-oil combustion, and industrial source. This factor also mapped to itself in all 100 bootstrap runs, with its base-run profile falling within the bootstrap interquartile range for 13 of 24 species.

Factor 3 accounted for 35.1% of the modelled elemental mass and was dominated by Ce (63.8%), Ba (62.4%), La (62.1%), and crustal elements including Ti (56.3%), Fe (53.1%), Si (48.2%), and Ca (37.8%). The combination of Ti, Fe, Si, and Ca indicates a strong crustal and road-dust component, while Ce, La, and Ba may reflect traffic-related abrasion and vehicle-related emissions [15]. The moderate S contribution (37.6%) may indicate some secondary sulfate influence. Factor 3 was accordingly assigned as crustal dust and traffic-related abrasion. This was the least uniquely determined factor of the wet-season solution: it mapped to Factor 1 in 12 of 100 bootstrap runs and to Factor 2 in a further three, and its base-run profile falls within the bootstrap interquartile range for 12 of 24 species. Its separation from the dominant mixed factor should therefore be regarded as partial.

Overall, the wet-season PMF solution was characterized by a dominant mixed regional factor (Factor 1), a smaller mixed combustion and traffic factor (Factor 2), and a crustal and traffic-related factor (Factor 3) whose separation from Factor 1 was only partially resolved. Compared with the dry season, the wet-season factors show greater mixing of source signatures, consistent with lower concentrations and stronger wet scavenging during the southwest monsoon.

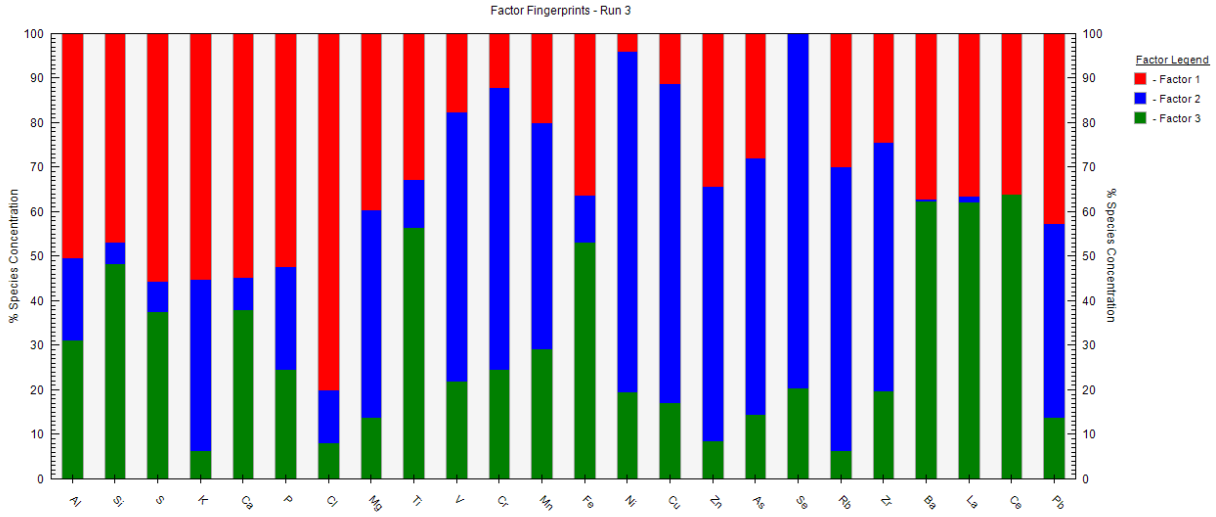

Figure 3. Factor fingerprints for the wet-season three-factor solution.

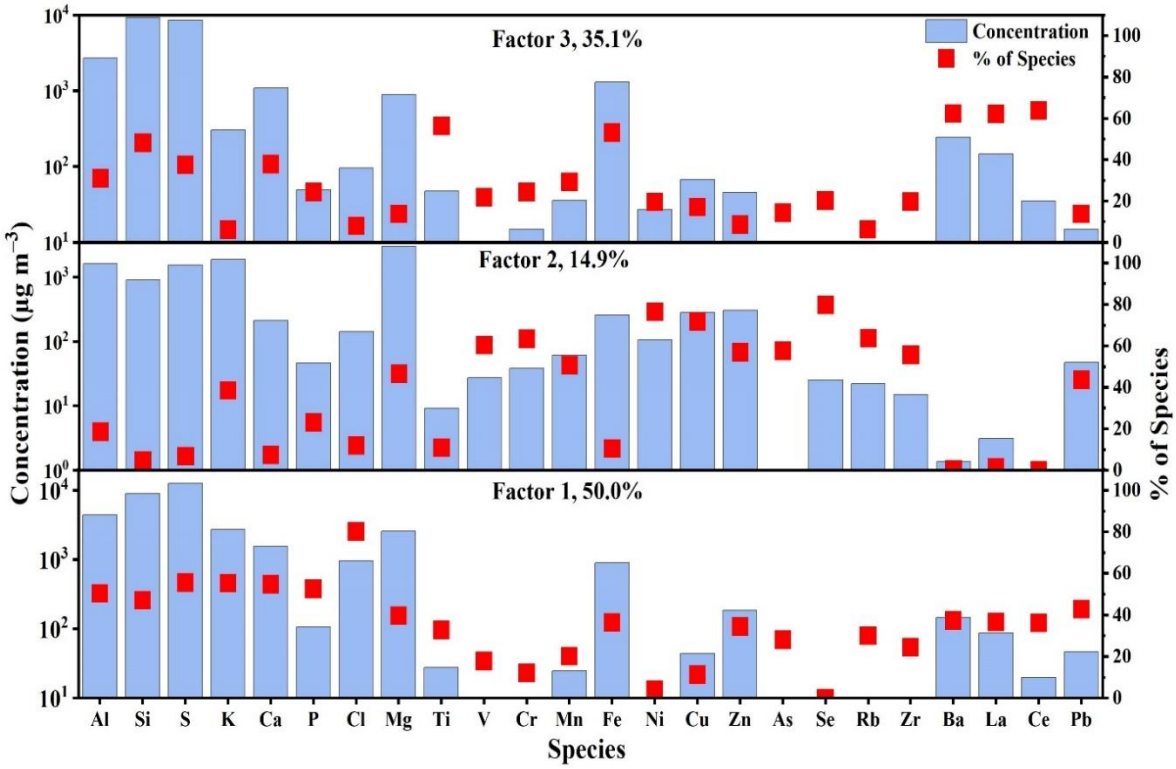

Figure 4. Source apportionment of $PM_{2.5}$ based on metal and elemental composition in the wet season using positive matrix factorization (PMF).

3.4 Comparison of seasonal source profiles

Comparison of the dry- and wet-season PMF solutions showed clear differences in source structure under the contrasting northeast and southwest monsoon conditions. Four factors were resolved during the dry season, compared with three during the wet season. Nevertheless, several major source characteristics were present in both seasons, including traffic-related emissions, combustion sources, and crustal material.

Factors carrying traffic-related and fuel-oil combustion tracers showed similar proportional contributions in the dry and wet seasons, accounting for 13.8% and 14.9% of the modelled elemental mass, respectively, although the wet-season factor also carried Se and As signatures. The presence of

Cu, Ni, and V in both seasonal solutions indicates the continued influence of local traffic-related non-exhaust emissions and residual fuel-oil combustion [15, 17, 18]. The similar absolute concentrations of Cu and Ni between seasons further suggest that these local sources persist throughout the year, although their relative importance within the modelled elemental mass increases when regional contributions decline in the wet season. This is the most robust of the seasonal comparisons presented here, as both factors met the error estimation criteria described in Section 2.4.

The tentatively identified industrial/metal-processing source and the coal/fuel-combustion source were more clearly separated during the dry season. Factor 1 was characterized by As and Pb, while Factor 2 was dominated by Se and S. In the wet season, these source signatures were not resolved as independent factors and were instead present together with traffic- and combustion-related elements in Factor 2. This greater mixing may reflect the lower concentrations and weaker source contrasts during the wet season [5]. The continued association of As, Se, and Pb with the wet-season factor suggests that these combustion and industrial influences were still present, although they were not sufficiently distinct to form separate factors, and the As contribution should be interpreted with caution given its low wet-season signal.

The dominant factors also differed substantially between seasons. Dry-season Factor 3 accounted for 46.9% of the modelled elemental mass and represented mixed urban and regional aerosol, with contributions from secondary sulfate, crustal material, traffic-related elements, and biomass burning. This profile is consistent with the stronger influence of regional transport and combustion during the northeast monsoon. In the wet season, Factor 1 was dominant, accounting for 50.0% of the modelled elemental mass, and showed a broad mixture of secondary, combustion, crustal, and marine-related elements. Its high share of Cl (80.1%), together with Mg, suggests a stronger marine influence during the southwest monsoon. The continued presence of S, K, and Rb indicates that secondary sulfate and biomass-burning influences remained detectable, although at lower absolute concentrations than during the dry season.

A notable difference was the resolution of a separate crustal and traffic-related factor during the wet season. Factor 3 accounted for 35.1% of the modelled elemental mass and was characterized by Ti, Fe, Si, and Ca together with Ce, La, and Ba. These elements indicate a combination of crustal or road dust and traffic-related abrasion. In the dry season, similar elements were distributed within the dominant mixed Factor 3, where their source signature was less clearly separated from the stronger regional, combustion, and biomass-burning influences. The resolution of this factor during the wet season suggests that local crustal and traffic-related sources may become more prominent within the elemental mass. As noted in Section 3.3, however, the wet-season crustal factor overlapped partially with the dominant factor in bootstrap analysis, so this represents a change in the resolvability of the signature rather than demonstrated evidence that the underlying source contribution itself increased.

Overall, the seasonal comparison indicates that the source mixture at the study site is strongly influenced by monsoon conditions. The dry season was characterized by stronger regional, biomass-burning, and combustion influences, with the industrial and coal/fuel combustion signatures more clearly separated. In contrast, the wet season showed greater mixing of combustion and traffic-related signatures, a stronger marine influence, and a separately resolved, though only partially distinct, crustal and traffic-related factor. These results demonstrate that seasonal meteorological conditions affect not only the magnitude of $PM_{2.5}$ concentrations but also the degree to which individual sources can be distinguished by receptor modelling.

3.5 Limitations

Each seasonal PMF solution was based on 62 daily samples and 24 species, which meets the minimum generally required for PMF but is modest for a complex urban airshed; the factor profiles therefore carry wide uncertainty, particularly in the dry season (Section 2.4), and individual factors are interpreted as composite signatures rather than discrete emission sources. Arsenic was retained as a

weak species with low signal-to-noise ratios (2.1 dry, 0.3 wet), and its wet-season values lay largely at the detection-limit substitution value, so As loadings provide only supporting evidence for the industrial attribution. Finally, the two 62-day windows represent the peak northeast and southwest monsoon regimes rather than the full annual cycle, because the April–June 2025 record failed quality control and the September–October transition period was excluded (Section 2.2); the reported contributions should therefore not be interpreted as annual mean source contributions.

4. CONCLUSIONS

Hourly $PM_{2.5}$ and elemental concentrations measured by automated XRF at an urban site in central Bangkok showed a significant threefold seasonal difference in $PM_{2.5}$, from 33.9 μg m^{-3} in the dry season (December 2024-January 2025) to 11.0 μg m^{-3} in the wet season (July-August 2025), with the dry-season mean exceeding the WHO 24-h guideline. K, S and Rb were enhanced 3.8- to 4.6-fold in the dry season, consistent with regional biomass burning and secondary aerosol, whereas Cu and Ni showed little seasonal variation, indicating persistent local sources.

PMF resolved four factors in the dry season and three in the wet season. A mixed traffic and fuel-oil combustion factor contributed similarly in both seasons (13.8% and 14.9% of the modelled elemental mass) and was the most robust finding of the study. The industrial and coal/fuel combustion signatures separated in the dry season were combined with other sources in the wet season, while a crustal dust and traffic-abrasion factor (35.1%) was resolved only in the wet season, although its separation from the dominant factor was partial. These results indicate that monsoon conditions affect both $PM_{2.5}$ levels and the degree to which sources can be separated by receptor modelling. Because they are based on two monsoon-peak windows, longer records covering the inter-monsoon periods are recommended to confirm these source attributions.

Acknowledgement

We thank the Department of Environmental and Sustainable Engineering, Faculty of Engineering, Chulalongkorn University, for providing monitoring site and sampling data.

References

[1] Global burden of 87 risk factors in 204 countries and territories, 1990-2019: a systematic analysis for the Global Burden of Disease Study 2019. (2020). *Lancet*, *396*(10258), 1223-1249. https://doi.org/10.1016/s0140-6736(20)30752-2

[2] Organization, W. H. (2021). *WHO global air quality guidelines: particulate matter (PM2. 5 and PM10), ozone, nitrogen dioxide, sulfur dioxide and carbon monoxide: executive summary*. World Health Organization.

[3] Thurston, G. D., Kipen, H., Annesi-Maesano, I., Balmes, J., Brook, R. D., Cromar, K., De Matteis, S., Forastiere, F., Forsberg, B., Frampton, M. W., Grigg, J., Heederik, D., Kelly, F. J., Kuenzli, N., Laumbach, R., Peters, A., Rajagopalan, S. T., Rich, D., Ritz, B.,…Brunekreef, B. (2017). A joint ERS/ATS policy statement: what constitutes an adverse health effect of air pollution? An analytical framework. *European Respiratory Journal*, *49*(1), 1600419. https://doi.org/10.1183/13993003.00419-2016

[4] Kelly, F. J., & Fussell, J. C. (2012). Size, source and chemical composition as determinants of toxicity attributable to ambient particulate matter. *Atmospheric Environment*, *60*, 504-526. https://doi.org/https://doi.org/10.1016/j.atmosenv.2012.06.039

[5] Viana, M., Kuhlbusch, T. A. J., Querol, X., Alastuey, A., Harrison, R. M., Hopke, P. K., Winiwarter, W., Vallius, M., Szidat, S., Prévôt, A. S. H., Hueglin, C., Bloemen, H., Wåhlin, P., Vecchi, R., Miranda, A. I., Kasper-Giebl, A., Maenhaut, W., & Hitzenberger, R. (2008). Source apportionment of particulate matter in Europe: A review of methods and results. *Journal of Aerosol Science*, *39*(10), 827-849. https://doi.org/https://doi.org/10.1016/j.jaerosci.2008.05.007

[6] Norris, G., Duvall, R., Brown, S., & Bai, S. (2014). EPA positive matrix factorization (PMF) 5.0 fundamentals and user guide, US Environmental Protection Agency, Washington, DC. In: EPA/600/R-14/108 (NTIS PB2015-105147), https://cfpub. epa. gov/si

[7] Paatero, P., & Tapper, U. (1994). Positive matrix factorization: A non-negative factor model with optimal utilization of error estimates of data values. *Environmetrics*, *5*(2), 111-126. https://doi.org/https://doi.org/10.1002/env.3170050203

[8] Ahmad, M., Thaveevong, P., Aman, N., Ngamsritrakul, T., & Panyametheekul, S. (2025). The PM2. 5-bound metals in the metropolitan area of Bangkok, Thailand: Temporal trends, sources, and human health challenges. *Environmental Challenges*, *18*, 101092.

[9] Ahmad, M., Panyametheekul, S., Thaveevong, P., Ngamsritrakul, T., Tassaneetrithep, B., Supasri, T., & Bennett, C. (2025). Long-term monitoring of PM2.5 and PM10: Implications for air quality and public health in urban Bangkok, Thailand. *Environmental Challenges*, *21*, 101312. https://doi.org/https://doi.org/10.1016/j.envc.2025.101312

[10] Ratanavalachai, T., & Trivitayanurak, W. (2023). Application of a PM2.5 dispersion model in the Bangkok central business district for air quality management [Original Research]. *Frontiers in Environmental Science*, *Volume 11 - 2023*. https://doi.org/10.3389/fenvs.2023.1237366

[11] Amphalop, S., Chienthavorn, O., Meesat, R., Tangpong, P., Chutichaisakda, M., Manohar, M., Wilkins, F., & Sudprasert, W. (2023). Source identification of PM2.5 during the COVID-19 lockdown in Bangkok and the metropolitan region by ion beam analysis (IBA) and positive matrix factorization (PMF) techniques. *Atmospheric Pollution Research*, *14*(7), 101814. https://doi.org/https://doi.org/10.1016/j.apr.2023.101814

[12] Kanchanasuta, S., Sooktawee, S., Patpai, A., & Vatanasomboon, P. (2020). Temporal Variations and Potential Source Areas of Fine Particulate Matter in Bangkok, Thailand. *Air, Soil and Water Research*, *13*, 1178622120978203. https://doi.org/10.1177/1178622120978203

[13] Narita, D., Oanh, N. T. K., Sato, K., Huo, M., Permadi, D. A., Chi, N. N. H., Ratanajaratroj, T., & Pawarmart, I. (2019). Pollution Characteristics and Policy Actions on Fine Particulate Matter in a Growing Asian Economy: The Case of Bangkok Metropolitan Region. *Atmosphere*, *10*(5), 227. https://www.mdpi.com/2073-4433/10/5/227

[14] Polissar, A. V., Hopke, P. K., Paatero, P., Malm, W. C., & Sisler, J. F. (1998). Atmospheric aerosol over Alaska: 2. Elemental composition and sources. *Journal of Geophysical Research: Atmospheres*, *103*(D15), 19045-19057. https://doi.org/10.1029/98jd01212

[15] Grigoratos, T., & Martini, G. (2014). Brake wear particle emissions: a review. *Environmental science and pollution research international*, *22*. https://doi.org/10.1007/s11356-014-3696-8

[16] Thongsame, W., Henze, D. K., Barth, M., Pfister, G., Kumar, R., Macatangay, R., & Hassan Bran, S. (2025). Source Attribution and Health Burden of PM(2.5) in Mainland Thailand. *Geohealth*, *9*(9), e2024GH001315. https://doi.org/10.1029/2024gh001315

[17] Brezins, M., Chazeau, B., Marchand, N., Gille, G., Soubise, J., Favez, O., Jaffrezo, J. L., Uzu, G., & D'Anna, B. (2026). Evolution of the V/Ni Ratio in Response to IMO Regulation-Induced Fuel Shifts and Scrubber Use. *Environmental Science & Technology Letters*, *13*(4), 516-523. https://doi.org/10.1021/acs.estlett.5c01199

[18] Yu, G., Zhang, Y., Yang, F., He, B., Zhang, C., Zou, Z., Yang, X., Li, N., & Chen, J. (2021). Dynamic Ni/V Ratio in the Ship-Emitted Particles Driven by Multiphase Fuel Oil Regulations in Coastal China. *Environmental Science & Technology*, *55*. https://doi.org/10.1021/acs.est.1c02612